

The high-redshift star formation rate derived from GRBs: possible origin and cosmic reionization

F. Y. Wang^{1,2,3}

¹ School of Astronomy and Space Science, Nanjing University, Nanjing 210093, China;

² Department of Physics, The University of Hong Kong, Pokfulam Road, Hong Kong, China;

³ Key Laboratory of Modern Astronomy and Astrophysics (Nanjing University), Ministry of Education, Nanjing 210093, China;

Preprint online version: January 24, 2014

ABSTRACT

The collapsar model of long gamma-ray bursts (GRBs) indicates that they may trace the star formation history. So long GRBs may be a useful tool of measuring the high-redshift star formation rate (SFR). The collapsar model explains GRB formation via the collapse of a rapidly rotating massive star with $M > 30M_{\odot}$ into a black hole, which may imply a decrease of SFR at high redshift. However, we find that the *Swift* GRBs during 2005-2012 are biased tracing the SFR, including a factor about $(1+z)^{0.5}$, which is in agreement with recent results. After taking this factor, the SFR derived from GRBs does not show steep drop up to $z \sim 9.4$. We consider the GRBs produced by rapidly rotating metal-poor stars with low masses to explain the high-redshift GRB rate excess. The chemically homogeneous evolution scenario (CHES) of rapidly rotating stars with mass larger than $12M_{\odot}$ is recognized as a promising path towards collapsars in connection with long GRBs. Our results indicate that the stars in the mass range $12M_{\odot} < M < 30M_{\odot}$ for low enough metallicity $Z \leq 0.004$ with the GRB efficiency factor 10^{-5} can fit the derived SFR with good accuracy. Combining these two factors, we find that the conversion efficiency from massive stars to GRBs is enhanced by a factor of 10, which may be able to explain the excess of the high-redshift GRB rate. We also investigate the cosmic reionization history using the derived SFR. The GRB-inferred SFR would be sufficient to maintain cosmic reionization over $6 < z < 10$ and reproduce the observed optical depth of Thomson scattering to the cosmic microwave background.

Key words. gamma-ray burst: general - stars: formation - reionization

1. Introduction

Gamma-ray bursts (GRBs) are the brightest electromagnetic explosions in the universe (for a recent review, see Gehrels et al. 2009). Because of their very high luminosity, GRBs can be detected out to the edge of the visible Universe (Ciardi & Loeb 2000; Lamb & Reichart 2000; Bromm & Loeb 2002, 2006). The farthest GRB to date is GRB 090429B with a photometric redshift $z = 9.4$ (Cucchiara et al. 2011), significantly larger than those of the most distant quasars. This property makes GRBs indispensable beacons to study the early universe, including the star formation rate (Totani 1997; Wijers et al. 1998; Porciani & Madau 2001; Bromm & Loeb 2002, 2006), the intergalactic medium (IGM) (Barkana & Loeb 2004; Inoue et al. 2007; McQuinn et al. 2008), and the metal enrichment history (Savaglio 2006; Wang et al. 2012). In addition, GRBs have been used as standard candles to constrain cosmological parameters and dark energy (Dai, Liang & Xu 2004; Schaefer 2007; Wang, Qi & Dai 2011).

The most popular theoretical model of long-duration GRBs is the collapse of a massive star to a black hole (Woosley 1993). Observations also show that GRBs are associated with Type Ib/c supernovae (Stanek et al. 2003; Hjorth et al. 2003). So GRBs provide a complementary technique for measuring the SFR history (Totani 1997; Wijers et al. 1998; Porciani & Madau 2001). Recent studies show that *Swift* GRBs are not tracing the star formation history measured by traditional means exactly but including an additional evolution (Le & Dermer 2007; Salvaterra & Chincarini 2007; Kistler et al. 2008; Yüksel et al. 2008; Wang & Dai 2009; Wanderman, & Piran 2010; Qin et al. 2010; Cao et

al. 2011; Robertson & Ellis 2012; but see Elliott et al. 2012). The SFR inferred from the high-redshift ($z > 6$) GRBs seems to be too high in comparison with the one obtained from some high-redshift galaxy surveys (Kistler et al. 2009; Bouwens et al. 2009). Kistler et al. (2008) found that there are about four times as many GRBs at redshift $z \sim 4$ than expected from star formation measurements. They claimed that some unknown mechanism is leading to an enhancement about $(1+z)^{\delta}$ ($\delta = 1.5$) in the observed rate of high-redshift GRBs. Using more *Swift* data, Kistler et al. (2009) found a slightly lower value of enhancement about $(1+z)^{1.2}$. Robertson & Ellis (2012) found the value of δ is about 0.5 by comparing the cumulative redshift distribution of GRBs and SFR. But on the other hand, Elliott et al. (2012) found that the value of δ is about zero using a small sample of GRBs. In order to explain this discrepancy, many models have been proposed. Li (2008) explained the observed discrepancy between the GRB rate history and the star formation rate history as being due to cosmic metallicity evolution (Langer & Norman 2006), by assuming that long GRBs tend to occur in galaxies with low metallicities. Cheng et al. (2010) suggested that this discrepancy could be solved if some high-redshift GRBs are produced by superconducting cosmic strings. Wang & Dai (2011) used an evolving initial mass function (IMF) of stars to explain the GRB redshift distribution. Virgili et al. (2011) discussed the possibility that the evolution of the GRB luminosity function break with redshift may explain this discrepancy. Observations also show differences in the population of GRB host galaxies compared to expectations for an unbiased star-formation tracer (Tanvir et al. 2004; Fruchter et al. 2006; Svensson et al. 2010).

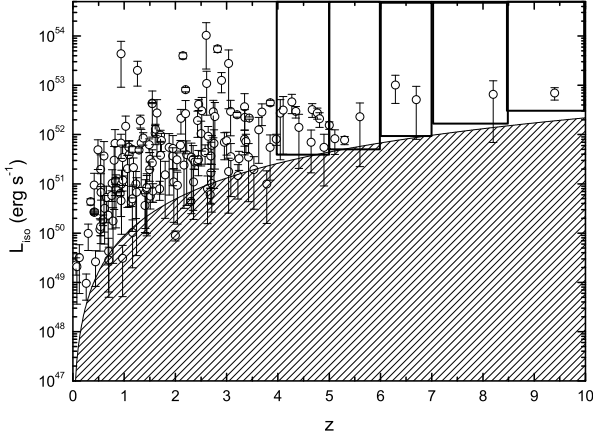


Fig. 1: Distribution of the isotropic-equivalent luminosity for 157 long-duration *Swift* GRBs. Demarcated are the GRB subsamples used to estimate the SFR. The shaded area approximates the detection threshold of *Swift* BAT.

In this paper, we study the star formation rate history derived from GRBs. First we use the *Swift* GRB sample to test the evolution of GRB rate relative to SFR. If GRBs trace star formation in the universe without bias, the ratio of the GRB rate to the SFR would not be expected to vary with redshift. We find that this ratio is proportional to $(1+z)^{0.5}$. The index is smaller than the value of Kistler et al. (2009). We also derive the high-redshift SFR using *Swift* GRB sample by correcting this evolution. Then, we consider the rapidly rotating metal-poor stars with masses smaller than critical mass $M_{\text{cri}} \sim 30M_{\odot}$ to see if they can produce GRBs to explain the discrepancy between high-redshift SFR and GRB rate. The collapsar model indicates that stars with mass larger than $30M_{\odot}$ can produce GRBs (Woosley 1993; Bissaldi et al. 2007; Raskin et al. 2008). Observation also shows that the progenitor of GRB 060505 has a mass above $30M_{\odot}$ (Thöne et al. 2008). Yoon & Langer (2005) investigated the evolution of rotating single stars in the mass range $12M_{\odot} < M < 60M_{\odot}$ at low metallicity. They found that if the initial spin rate is high enough, the time scale for rotationally induced mixing becomes shorter than the nuclear time scale. The star may evolve in a quasi-chemically homogeneous way. In particular, for low enough metallicity, this type of evolution can lead to retention of sufficient angular momentum in cores to produce GRBs according to the collapsar scenario. Last, we calculate the impact of this GRB-inferred star formation rate on the reionization history, including the optical depth of electron scattering to the cosmic microwave background.

The structure of this paper is arranged as follows. In the next section, we compile the *Swift* GRB sample till GRB 110403 and test the evolution of GRB rate. The SFR derived from GRBs is given in section 3. We show the model of GRBs from chemically homogeneous evolution scenario and the influence on high-redshift SFR derived from GRBs in section 4. We compute the reionization history with this GRB-inferred SFR in section 5. We conclude with a summary in section 6.

2. The latest GRB sample

The expected redshift distribution of GRBs is

$$\frac{dN}{dz} = F(z) \frac{\epsilon(z) \dot{\rho}_*(z)}{\langle f_{\text{beam}} \rangle} \frac{dV_{\text{com}}/dz}{1+z}, \quad (1)$$

where $F(z)$ represents the ability both to detect the trigger of burst and to obtain the redshift, $\epsilon(z)$ accounts for the fraction of stars producing GRBs, $\dot{\rho}_*(z)$ is the SFR density. The $F(z)$ can be treated as constant when we consider the bright bursts with luminosities sufficient to be detected within an entire redshift range, so $F(z) = F_0$. GRBs that are unobservable due to beaming are accounted for through $\langle f_{\text{beam}} \rangle$. The $\epsilon(z)$ can be parameterized as $\epsilon(z) = \epsilon_0(1+z)^{\delta}$, where ϵ_0 is an unknown constant that includes the absolute conversion from the SFR to the GRB rate in a given GRB luminosity range. Kistler et al. (2008) found the index $\delta = 1.5$ from 63 *Swift* GRBs. A little smaller value $\delta = 1.2$ was inferred using 119 *Swift* GRBs (Kistler et al. 2009). In a flat universe, the comoving volume is calculated by

$$\frac{dV_{\text{com}}}{dz} = 4\pi D_{\text{com}}^2 \frac{dD_{\text{com}}}{dz}, \quad (2)$$

where the comoving distance is

$$D_{\text{com}}(z) \equiv \frac{c}{H_0} \int_0^z \frac{dz'}{\sqrt{\Omega_m(1+z')^3 + \Omega_{\Lambda}}}. \quad (3)$$

In the calculations, we use $\Omega_m = 0.27$, $\Omega_{\Lambda} = 0.73$ and $H_0 = 71 \text{ km s}^{-1} \text{ Mpc}^{-1}$ from the *Wilkinson Microwave Anisotropy Probe* (WMAP) seven-year data (Komatsu et al. 2011).

We use the latest *Swift* long-duration GRB sample till GRB 110403. The data is taken from Butler et al. (2007, 2010) and website¹. The isotropic-equivalent luminosity of a GRB can be obtained by

$$L_{\text{iso}} = E_{\text{iso}}(1+z)/T_{90}. \quad (4)$$

The distribution of L_{iso} for 157 GRBs in the sample is shown in Figure 1. We use the same luminosity cuts in these redshift bins as Kistler et al. (2009). The shaded area approximates the detection threshold of *Swift* BAT, which can be calculated as follows. The luminosity threshold can be approximated by a bolometric energy flux limit $F_{\text{lim}} = 1.2 \times 10^{-8} \text{ erg cm}^{-2} \text{ s}^{-1}$. The luminosity threshold is then

$$L_{\text{lim}} = 4\pi D_L^2 F_{\text{lim}}, \quad (5)$$

where D_L is the luminosity distance to the burst.

In order to test the GRB rate relative to the SFR, we must choose bursts with high luminosities, because only bright bursts can be seen at low and high-redshifts, so we choose the luminosity cut $L_{\text{iso}} > 10^{51} \text{ erg s}^{-1}$ (Yüksel et al. 2008) in the redshift bin 0–4. This removes many low-redshift, low- L_{iso} bursts that could not have been seen at higher redshift. Because the SFR at high redshift is poorly known (Bouwens et al. 2012; Oesch et al. 2013; Coe et al. 2013), so we choose the redshift range $0 < z < 4$, in which SFR is well measured. We have 92 GRBs in this subsample. We use the SFR history from Hopkins & Beacom (2006). We compare the predicted and observed cumulative GRB distributions in Figure 2. We find that the Kolmogorov-Smirnov statistic is minimized for $\delta = 0.5$, which is consistent with Robertson & Ellis (2012). At the 2σ confidence level, the value of δ is in the range $-0.15 < \delta < 1.6$.

¹ http://astro.berkeley.edu/~nat/Swift/bat_spec_table.html

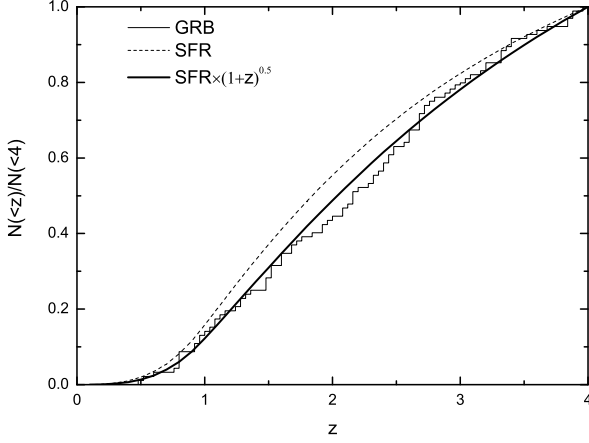


Fig. 2: Cumulative distribution of 92 *Swift* GRBs with $L_{\text{iso}} > 10^{51} \text{ erg s}^{-1}$ in $z = 0 - 4$ (stepwise solid line). The dashed line shows the GRB rate inferred from the star formation history of Hopkins & Beacom (2006). The solid line shows the GRB rate inferred from the star formation history including $(1+z)^{0.5}$ evolution.

Our result is smaller than the values in Kistler et al. (2009). This may be account for the different GRB sample. The GRB sample observed by *Swift* during 2005-2012 is used in this paper. This bias must be taken into account when one relates the GRB rate to the SFR.

3. The SFR derived from GRBs

In this section, we use the same method as Yüksel et al. (2008) to calculate the SFR rate from GRBs. Because only very bright bursts can be seen from all redshifts, we use the same luminosity cuts as Kistler et al. (2009), as shown in Figure 1. The number counts in redshift bins $z = 4-5, 5-6, 6-7, 7-8.5$ and $8.5-10$ are 10, 4, 2, 1 and 1 respectively. In the redshift bin of $8.5-10$, there is only one GRB named GRB 090429B with photometric redshift $z \sim 9.4$, although there is a low-probability tail to somewhat lower redshifts (Cucchiara et al. 2011). The bin choice of this work is different with those of Robertson & Ellis (2012). In this work, we choose redshift bins uniform in z , and also ensure that the number of GRBs in each bins is equal or larger than one. We also calculate the SFR using bin choice of Robertson & Ellis (2012), and find that the result is a little difference compared with current bin choice. The GRBs in $z = 1-4$ act as a “control group” to constrain the GRB to SFR conversion, since this redshift bin has both good SFR measurements and GRB counts. We calculate the theoretically predicated number of GRBs in this bin as

$$N_{1-4}^{\text{the}} = \Delta t \frac{\Delta \Omega}{4\pi} \int_1^4 dz F(z) \epsilon(z) \frac{\dot{\rho}_*(z)}{\langle f_{\text{beam}} \rangle} \frac{dV_{\text{com}}/dz}{1+z} \\ = A \int_1^4 dz (1+z)^\delta \dot{\rho}_*(z) \frac{dV_{\text{com}}/dz}{1+z}, \quad (6)$$

where $A = \Delta t \Delta \Omega F_0 / 4\pi \langle f_{\text{beam}} \rangle$ depends on the total observed time of *Swift*, Δt , and the angular sky coverage, $\Delta \Omega$. The theoretical number of GRBs in redshift bin $z_1 - z_2$ can be written

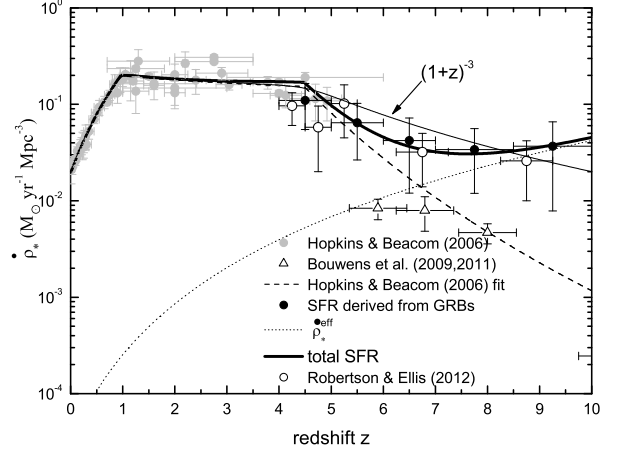


Fig. 3: The cosmic star formation history. The grey points are taken from Hopkins & Beacom (2006), the dashed line shows their fitting result. The triangular points are from Bouwens et al. (2009, 2011). The open circles are taken from Robertson & Ellis (2012). The filled circles are the SFR derived from GRBs in this work. The dotted line shows the effect SFR calculated from equation (19). The thick solid line shows the combination of dashed and dotted lines.

by

$$N_{z_1-z_2}^{\text{th}} = \langle \dot{\rho}_* \rangle_{z_1-z_2} A \int_{z_1}^{z_2} dz (1+z)^\delta \frac{dV_{\text{com}}/dz}{1+z}, \quad (7)$$

where $\langle \dot{\rho}_* \rangle_{z_1-z_2}$ is the average SFR density in the redshift range $z_1 - z_2$. Representing the predicated numbers, $N_{z_1-z_2}^{\text{th}}$ with the observed GRB counts, $N_{z_1-z_2}^{\text{obs}}$, we obtain the SFR in the redshift range $z_1 - z_2$,

$$\langle \dot{\rho}_* \rangle_{z_1-z_2} = \frac{N_{z_1-z_2}^{\text{obs}}}{N_{1-4}^{\text{obs}}} \frac{\int_1^4 dz \frac{dV_{\text{com}}/dz}{1+z} (1+z)^\delta \dot{\rho}_*(z)}{\int_{z_1}^{z_2} dz \frac{dV_{\text{com}}/dz}{1+z} (1+z)^\delta}. \quad (8)$$

In the calculation, we assume that the value of δ is constant at all redshift range. The derived SFR from GRBs are shown as filled circles in Figure 3. Error bars correspond to 68% Poisson confidence intervals for the binned events (Gehrels 1986). The high-redshift SFRs obviously decrease with increasing redshifts, although an oscillation may exist. We find that the SFR at $z > 4.48$ is proportional to $(1+z)^{-3}$ using minimum χ^2 method, which is shown as solid line in Figure 3. Because we use different cosmological parameters comparing to Hopkins & Beacom (2006) ($\Omega_m = 0.3, \Omega_\Lambda = 0.7$ and $H_0 = 70 \text{ km s}^{-1} \text{ Mpc}^{-1}$), SFR conversion between different cosmology models must be considered. The conversion factor for a given redshift range can be expressed as (Hopkins 2004)

$$\dot{\rho}_*(z) \propto \frac{D_{\text{com}}^2(z)}{D_{\text{com}}^3(z + \Delta z) - D_{\text{com}}^3(z - \Delta z)}, \quad (9)$$

where D_{com} is given in equation (3). At the redshift range $z = 4-5$, the value of conversion factors in these two cosmological models are very similar. The relative error is less than 4%. So our results are insensitive to the choice of WMAP7 cosmology.

The new determination of SFR is slight smaller than the result given by Kistler et al. (2009). There are two reasons for this situation. First, we derive a smaller evolution factor index δ . Second, we update the *Swift* GRB sample. In past three years, *Swift* has observed much more GRBs with medium redshifts than GRBs with high redshifts. So the ratio $N_{z_1-z_2}^{\text{obs}}/N_{1-4}^{\text{obs}}$ is smaller compared with Kistler et al. (2009).

Ishida et al. (2011) used the principal component analysis method to measure the high-redshift SFR from the distribution of GRBs and found that the SFR at $z \sim 9.4$ could be up to $0.01 M_{\odot} \text{ yr}^{-1} \text{ Mpc}^{-3}$. Robertson & Ellis (2012) constrained the SFR using GRBs by considering the contribution of “dark” GRBs. They found that the high-redshift SFR derived from GRBs can vary a factor of 4 using different values of δ . Their results for $\delta = 0.5$ are shown as open circles in Figure 3. Our results can be marginally consistent with the open dots. Elliott et al. (2012) chose 43 GRBs by selecting GRBs that have been detected by GROND within 4 hours after the Swift BAT trigger and that exhibited an X-ray afterglow. They found that the linear relationship between GRB rate and SFR using this small sample. Johnson et al. (2013) used high-resolution cosmological simulations to study the high-redshift SFR. Our result is consistent with that of Johnson et al. (2013) at $z \leq 10$. But at $z \geq 10$, they found the SFR is reduced by up to an order of magnitude due to the molecule-dissociating stellar radiation.

4. GRBs from rapidly rotating metal-poor stars and influence on SFR

The collapsar model explains GRB formation via the collapse of a rapidly rotation massive iron core into a black hole (Woosley 1993). This collapse model requires the initial mass of the massive stars with masses larger than about $30 M_{\odot}$ (Woosley 1993; Bissaldi et al. 2007). Yoon & Langer (2005) and Woosley & Heger (2006) showed that at low metallicity, quasi-chemically-homogeneous evolution of rapidly rotating stars with low masses can lead to the formation of rapidly rotating helium stars which satisfy all the requirements of the collapsar scenario. Because the rotation affects the evolution of stars significantly, especially through rotationally induced chemical mixing (Maeder & Meynet 2000; Heger et al. 2000). The star remains chemically homogeneous evolution scenario (CHES). The CHES is recognized as a promising path towards collapsars in connection with long GRBs. Yoon, Langer & Norman (2006) showed that at low metallicity ($Z \leq 0.004$), quasi-chemically-homogeneous evolution of rapidly rotating stars with masses larger than $12 M_{\odot}$ can lead to long GRBs². We call this type of GRBs as chemically homogeneous GRBs (CHG) below. If stars in the same mass range have high metallicities and slow rotation, they will die as type II supernovae (see Figure 3 of Yoon et al. 2006). This picture has also been confirmed by observation (Fruchter et al 2006).

We study the rate of CHG from chemically homogeneous evolution scenario as follows. The most widely used functional form for the initial mass function (IMF) is that proposed by Salpeter (1955):

$$\phi(M) = A_{\text{Salpeter}} M^{-2.35}, \quad (10)$$

² Although the lower limit mass of a star with low metallicity that can collapse to GRB is uncertain. But this value is unimportant in our analysis. The best fitting parameters will shift slightly when the lower limit mass is changed.

where $A_{\text{Salpeter}} = 0.06$ is the normalization constant derived from,

$$\int_{m_{\text{low}}}^{m_{\text{up}}} \phi(M) dM = 1. \quad (11)$$

We use $m_{\text{low}} = 0.1 M_{\odot}$ and $m_{\text{up}} = 120 M_{\odot}$. We consider stars with masses between $12 M_{\odot}$ and $30 M_{\odot}$. Because the stars with masses $M \geq 30 M_{\odot}$ can produce GRBs through conventional collapse model (Woosley 1993). So the rate of CHG is

$$R_{\text{CHG}} = k_{\text{CHG}} \Sigma(Z_{\text{th}}, z) \dot{\rho}_*(z) P(x > x_{\text{cr}}) \int_{12 M_{\odot}}^{30 M_{\odot}} \phi(M) dM, \quad (12)$$

where k_{CHG} with value about 10^{-5} is the CHGs formation efficiency, $\Sigma(Z_{\text{th}}, z)$ and $P(x > x_{\text{cr}})$ are discussed below. According to Langer & Norman (2006), the fractional mass density belonging to metallicity below a given threshold Z_{th} is

$$\Sigma(Z_{\text{th}}, z) = \frac{\hat{\Gamma}[\alpha_1 + 2, (Z_{\text{th}}/Z_{\odot})^2 10^{0.15\beta z}]}{\Gamma(\alpha_1 + 2)}, \quad (13)$$

where $\hat{\Gamma}$ and Γ are the incomplete and complete gamma functions, $\alpha_1 = -1.16$ is the power-law index in the Schechter distribution function of galaxy stellar masses (Panter, Heavens & Jimenez 2004) and $\beta = 2$ is the slope of the galaxy stellar mass-metallicity relation (Savaglio et al. 2005; Langer & Norman 2006). We extrapolate the metallicity evolution up to redshift $z \sim 9.4$. Observation shows that this metallicity evolution can be used up to $z \sim 3$ (Kewley & Kobulnicky 2007). This extrapolation has been widely used in literature (Langer & Norman 2006; Li 2008; Robertson & Ellis 2012). We set $Z_{\text{th}} = 0.004$. As discussed by Yoon, Langer & Norman (2006), the GRB production in CHES is limited to metallicity $Z_{\text{th}} \leq 0.004$. Within the CHES, the fraction of stars which forms a long GRB depends on the semi-convective mixing, and the distribution function of initial stellar rotation velocities, $D(v_{\text{init}}/v_K)$, where v_{init} is the initial rotation velocity and v_K is the Keplerian velocity. We use the v_{init}/v_K distribution from Yoon, Langer & Norman (2006)

$$D(x) = B \frac{\lambda^v}{\Gamma(v)} x^{v-1} \exp(-\lambda x), \quad (14)$$

where $\lambda = 9.95$, $v = 2$ and $x \equiv v_{\text{init}}/v_K$. The normalization constant $B = 3.2 \times 10^5$ is derived from $\int_0^{\infty} D(x) dx = 1$. They found that this distribution can fit well with the observational data from Mokiem et al. (2006). Figure 4 shows the numerical value of equation (14). In order to produce GRBs, the value of x should be larger than 0.4 (Yoon, Langer & Norman 2006), so $P(x > x_{\text{cr}}) = \int_{0.4}^{\infty} D(x) dx = 0.09$.

So the expected number of CHG between redshifts z and $z + \delta z$ can be calculated as

$$N_{\text{CHG}}^{\text{exp}}(>L) = F \Delta t \frac{\Delta \Omega}{4\pi} \int_z^{z+\delta z} dz \int_L^{\infty} dL \Phi(L) R_{\text{CHG}} \frac{dV_{\text{com}}/dz}{1+z}, \quad (15)$$

where $\Phi(L)$ is the luminosity function of GRBs. We use the Schechter-function form

$$\Phi(L) = \frac{1}{L_*} \left(\frac{L}{L_*} \right)^{\beta} \exp(-L/L_*), \quad (16)$$

where $\beta = -1.12$ and $L_* = 9 \times 10^{52} \text{ erg s}^{-1}$ (Wang & Dai 2011). The integral $\int_L^{\infty} dL \Phi(L)$ equals to $\Gamma(1 + \beta, \frac{L}{L_*})$, where Γ is the incomplete gamma function. Because $1 + \beta \rightarrow 0$, we can approximate $\Gamma(1 + \beta, \frac{L}{L_*}) \rightarrow -(\frac{L}{L_*})^{1+\beta}/(1 + \beta)$.

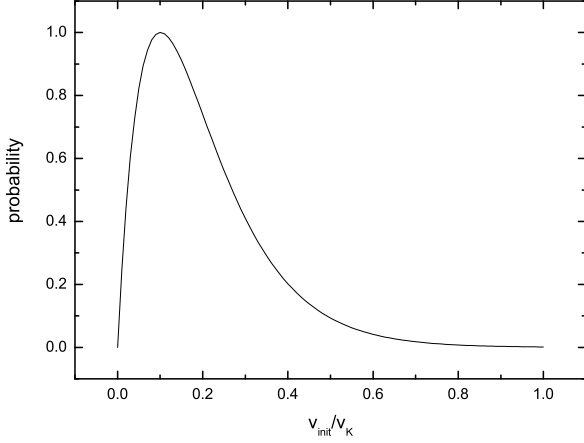


Fig. 4: Distribution of the initial rotation value of stars.

We define an effective SFR $\dot{\rho}_*^{\text{eff}}$, due to the CHG, as

$$\frac{N_{\text{CHG}}^{\text{exp}}(>L)}{N_{1-4}^{\text{obs}}(>L)} = \frac{\int_z^{z+\delta z} \epsilon \dot{\rho}_*^{\text{eff}} dV_{\text{com}}(z')/(1+z')}{\int_1^4 \epsilon \dot{\rho}_* dV_{\text{com}}(z')/(1+z')} \quad (17)$$

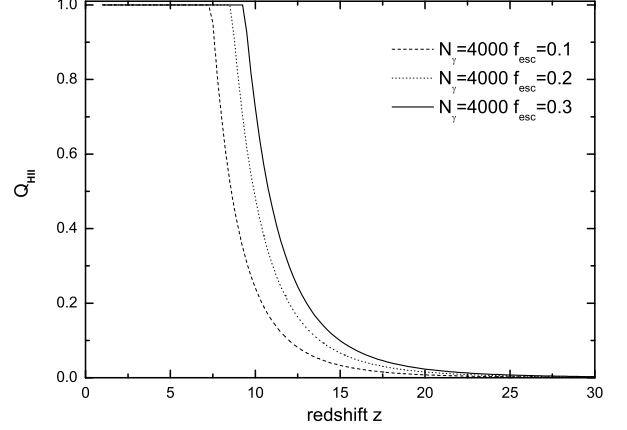
We consider the star formation history from Hopkins & Beacom (2006),

$$\dot{\rho}_*(z) \propto \begin{cases} (1+z)^{3.44}, & z < 0.97, \\ (1+z)^{-0.26}, & 0.97 < z < 4.48, \\ (1+z)^{-7.8}, & 4.48 < z. \end{cases} \quad (18)$$

with $\dot{\rho}_*(0) = 0.02 \text{ M}_{\odot} \text{ yr}^{-1} \text{ Mpc}^{-3}$. For convenience, here we fit the data by $N_{1-4}^{\text{obs}}(>L) \sim 60 L_{52}^{-\alpha}$ with $\alpha \sim 0.50$. Substituting Eq. (15) into Eq. (17), we can obtain the effective SFR as

$$\begin{aligned} \dot{\rho}_*^{\text{eff}} &= \frac{F_0 \Delta t \left(\frac{L_{\text{th}}}{L_*}\right)^{1+\beta} \int_1^4 \dot{\rho}_*(1+z)^{\delta-1} dV_{\text{com}} \frac{\Delta \Omega}{4\pi} R_{\text{CHG}}(>L_{\text{th}})}{(-1-\beta)(1+z)^{\delta} N_{1-4}^{\text{obs}}(>L_{\text{th}})} \\ &= C \text{ M}_{\odot} \text{ yr}^{-1} \text{ Mpc}^{-3} \int_{12M_{\odot}}^{30M_{\odot}} \phi(M) dM \rho_*(z) (1+z)_1^{1+\alpha-\delta+\beta} \\ &\quad \times \left(\frac{(1+z)^{1/2} - 1}{2} \right)^{2(\alpha+\beta+1)}, \end{aligned} \quad (19)$$

where the factor $C \sim 125 F_0 k_{\text{CHG},-5} F_{\text{lim},-8}^{1+\alpha+\beta}$. The luminosity threshold at redshift z can be calculated as $L_{\text{th}} = 4\pi D_L(z)^2 F_{\text{lim}}$ for a given flux sensitivity F_{lim} . For the *Swift* satellite, we adopt the angular sky coverage of $\Delta\Omega/4\pi \sim 0.1$, and the observation period $\Delta t \sim 7.5 \text{ yr}$. In equation (19), the integral $\int_{12M_{\odot}}^{30M_{\odot}} \phi(M) dM$ is proportional to $(12M_{\odot}^{-1.35} - 30M_{\odot}^{-1.35})/1.35 = 0.026$. Although there are many factors in equation (19) may subsume the effect in change the IMF integral for GRB production. The evolution of $\dot{\rho}_*^{\text{eff}}$ is shown as the dotted line in Figure 3. Bouwens et al. (2009, 2011) measured high-redshift SFR using color-selected Lyman break galaxies (LBGs) method. Their results are shown as triangular points in Figure 3. But LBG studies mainly probe the brightest galaxies. If the integration of UV luminosity functions down to $M_{UV} \simeq -10$, the SFR inferred from LBG is consistent with that derived


 Fig. 5: The HII filling factor Q_{HII} as a function of redshift computed for different values of f_{esc} .

from GRBs (Kistler et al. 2013). GRBs are found to favor sub-luminosity galaxies (Fynbo et al. 2003), so a larger fraction of the SFR within such hosts would be revealed by GRBs (Kistler et al. 2009). We can see that the SFR inferred from high-redshift GRBs can be well explained by combining equation (18) with equation (19) for $C \sim 125$. The overall conventional long GRB formation efficiency from massive stars is about $< 10^{-6}$ (Zitouni et al. 2008; Li 2008), which is smaller than k_{CHG} . This indicates that the subclass of massive stars with low metallicity and chemical homogeneity may produce long GRBs more efficiently.

5. Implications for the cosmic reionization

Determining when and how the universe was reionized by early sources have been important questions for decades (Gunn & Peterson 1965; Robertson et al. 2010). It is established that intergalactic medium (IGM) reionization may be completed by $z \approx 6.5$, based on strong Ly α absorption from neutral hydrogen along lines of sight to quasars at $z > 6$ (Fan et al. 2001). As a measure of ionization, we follow the evolution of the HII volume filling factor $Q_{\text{HII}} = n_e/n_H$, versus redshift, using the SFR derived from GRBs (the solid line in Figure 3). The average evolution of Q_{HII} is found by numerical integration of the rate of ionizing photons minus the rate of radiative recombinations (Madau et al. 1999; Barkana & Loeb 2001; Wyithe & Loeb 2003; Yu et al. 2012)

$$\frac{dQ_{\text{HII}}}{dz} = \left(\frac{\dot{N}_{\text{ion}}}{n_H} - \alpha_B C n_H Q_{\text{HII}} \right) \frac{dt}{dz}. \quad (20)$$

Here,

$$\dot{N}_{\text{ion}} = (1+z)^3 \dot{\rho}_*(z) N_{\gamma} f_{\text{esc}} / m_p \quad (21)$$

is the rate of ionizing UV photons escaping from the stars into the IGM, N_{γ} is the number of ionizing UV photons released per baryon of the stars, $(1+z)^3$ converts the comoving density into proper density, $\dot{\rho}_*(z)$ is proportional to $(1+z)^{-3}$ at $z > 4.48$ and f_{esc} is the escape fraction. The escape fraction is not well constrained. At low redshifts, observations show that the escape fraction from GRB hosts is about a few percent (Chen et al. 2007; Fynbo et al. 2009). But at high redshifts, the f_{esc} is larger

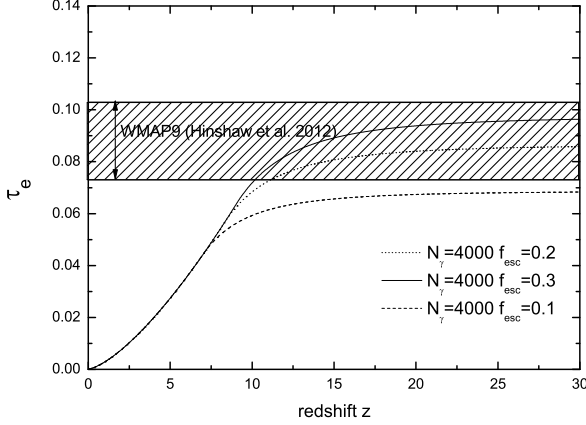


Fig. 6: The optical depth τ_e due to the scattering between the ionized gas and the CMB photons is shown. The shade region is given by the nine-year WMAP measurements ($\tau_e = 0.089 \pm 0.014$). The reionization history calculated from GRB-inferred SFR can easily reach τ_e from WMAP nine-year data.

(Inoue et al. 2005; Robertson et al. 2010). Recent estimates suggest that the clumping factor $C \approx 1 - 6$ (Bolton & Haehnelt 2007; Pawlik et al. 2009). We adopt $C = 3$ in this paper. n_H is the proper density of hydrogen, and $\alpha_B = 1.63 \times 10^{-13} \text{ cm}^3 \text{ s}^{-1}$ is the recombination rate for an electron temperature of about 10^4 K . Because the mass in collapsed objects is still small at high redshift, the IGM contains most of the cosmological baryons, at mean density

$$\rho_b = \Omega_b \rho_{\text{cr}} (1+z)^3 = 4.24 \times 10^{-31} (1+z)^3 \text{ g cm}^{-3}. \quad (22)$$

We adopt the parameters from WMAP seven-year, $\Omega_b h^2 = 0.02255 \pm 0.00054$ and $\Omega_m h^2 = 0.1352 \pm 0.0036$ (Komatsu et al. 2011). The critical density is $\rho_{\text{cr}} = 1.8785 \times 10^{-29} h^2 \text{ g cm}^{-3}$. The mean hydrogen number density,

$$n_H = \frac{\rho_b(1-Y)}{m_H} = 1.905 \times 10^{-7} (1+z)^3 \text{ cm}^{-3}, \quad (23)$$

where $Y = 0.2477 \pm 0.0029$ is the helium mass fraction (Peimbert et al. 2007). After the values of N_γ and f_{esc} are given, the evolution of the HII volume filling factor Q_{HII} can be numerically calculated from equation (20). In Figure 5, we show the evolution of Q_{HII} as a function of redshift. For $N_\gamma = 4000$ and $f_{\text{esc}} = 0.2$, the IGM was completely ionized at $z_{\text{rei}} \sim 8.5$.

The cosmic microwave background (CMB) optical depth back to redshift z can be written as the integral of $n_e \sigma_T d\ell$, the electron density times the Thomson cross section along proper length,

$$\tau_e(z) = \int_0^z n_e(z') \sigma_T (1+z')^{-1} [c/H(z')] dz'. \quad (24)$$

So after we obtain the redshift evolution of $n_e(z)$, the CMB optical depth as a function of redshift can be calculated. More recently, the Planck team has released the latest result on cosmological parameters (Planck Collaboration 2013). In the calculation, we extrapolate the SFR as $(1+z)^{-3}$ to $z \sim 30$. The first stars, so-called Population III (Pop III) stars are predicated to have formed at $z > 20$ in minihalos (Tegmark et al. 1997;

Yoshida et al. 2003). Heger et al. (2003) and Mészáros & Rees (2010) show that Pop III stars can die as GRBs. The formation rate of Pop III GRBs has been extensively studied (Campisi et al. 2011; de Souza et al. 2011). The high luminosities of GRBs make them detectable out to the edge of the visible universe (Bromm & Loeb 2002, 2006; Wang et al. 2012). So GRBs may provide the information of SFR out to $z > 20$ in future. The extrapolation of SFR to high redshifts may be reasonable. The optical depth is shown in Figure 6. The WMAP nine-year data gives $\tau_e = 0.089 \pm 0.014$ (Hinshaw et al. 2012), which is shown as the shaded region. The combination of Planck and WMAP data also gives $\tau_e = 0.089^{+0.012}_{-0.014}$ (Planck Collaboration 2013). So our GRB-inferred SFR can reproduce the CMB optical depth.

6. Summary

Using the GRB catalogs, we have constructed the cumulative redshift distribution of 110 luminous ($L_{\text{iso}} > 10^{51} \text{ erg s}^{-1}$) GRBs out to redshift $z \sim 9.4$. We find that the *Swift* GRBs during 2005-2012 are biased toward tracing the SFR, including a factor of about $(1+z)^{0.5}$. Correcting this evolution, we derive the star formation history up to $z \sim 9.4$ using *Swift* GRB sample. Our results show that no steep drop exists in the SFR up to at least $z \sim 9.4$. In order to explain the high-redshift GRB rate excess, the GRBs produced by rapidly rotating metal-poor stars with low mass are considered. The collapsar model explains GRB formation via the collapse of a massive star with $M > 30 M_\odot$ into a black hole. We consider that at low metallicity, quasi-chemically homogeneous evolution of rapidly rotating stars with mass larger than $12 M_\odot$ can lead to the formation of GRBs. The low metallicity and rapid rotation can lead to efficiently produce GRBs in two ways. First, rapid rotation keeps the stars chemically homogeneous and thus avoids the formation of a massive envelope, so stellar core is free of spin-down due to magnetic core-envelope coupling. Second, the stellar wind is weak at low metallicity, so this reduces spin-down due to stellar winds. Our fitting results confirm this idea. We also calculate the reionization history using the GRB-inferred SFR, and find that this SFR can maintain cosmic reionization over $6 < z < 10$ and reproduce the observed optical depth of Thomson scattering to the cosmic microwave background.

Acknowledgements. We thank the anonymous referee for very useful comments and suggestions. We thank K. S. Cheng and Z. G. Dai for fruitful discussion. We acknowledge the use of public data from the *Swift* data archive. This work is supported by the National Natural Science Foundation of China (grant 11103007 and 11033002).

References

- Barkana, R., & Loeb, A. 2001, *Phys. Rep.*, 349, 125
- Barkana, R., & Loeb, A. 2004, *ApJ*, 601, 64
- Bissaldi, E., Calura, F., Matteucci, F., Longo, F. & Barbiellini, G. 2007, *A&A*, 471, 585
- Bolton, J. S. & Haehnelt, M. G., 2007, *MNRAS*, 382, 325
- Bouwens, R. J., et al. 2009, *ApJ*, 705, 936
- Bouwens, R. J., et al. 2011, *Nature*, 469, 504
- Bouwens, R. J., Illingworth, G. D., Oesch, P. A., et al. 2012, *ApJ*, 752, L5
- Bromm, V., & Loeb, A. 2002, *ApJ*, 575, 111
- Bromm, V., & Loeb, A. 2006, *ApJ*, 642, 382
- Butler, N. R., Bloom, J. S., & Poznanski, D. 2010, *ApJ*, 711, 495
- Butler, N. R., Koevski, D., Bloom, J. S., & Curtis, J. L. 2007, *ApJ*, 671, 656
- Campisi, M. A., Maio, U., Salvaterra, R. & Ciardi, B. 2011, *MNRAS*, 416, 2760
- Cao, X. F., Yu, Y. W., Cheng, K. S. & Zheng, X. P. 2011, *MNRAS*, 416, 2174
- Chen, H. W., Prochaska, J. X. & Gnedin, N. Y., 2007, *ApJ*, 667, L125
- Cheng, K. S., Yu, Y., & Harko, T. 2010, *Phys. Rev. Lett.*, 104, 241102
- Ciardi, B., & Loeb, A. 2000, *ApJ*, 540, 687
- Coe, D., Zitrin, A., Carrasco, M., et al. 2013, *ApJ*, 762, 32

- Cucchiara, A. et al. 2011, *ApJ*, 736, 7
- Dai, Z. G., Liang, E. W., & Xu, D. 2004, *ApJ*, 612, L101
- de Souza, R. S., Yoshida, N. & Ioka, K. 2011, *A&A*, 533, A32
- Elliott, J., Greiner, J., Khochfar, S., Schady, P., Johnson, J. L. & Rau, A. 2012, *A&A*, 539, A113
- Fan, X., et al. 2001, *AJ*, 122, 2833
- Fruchter, A. S., et al. 2006, *Nature*, 441, 463
- Fynbo, J. P. U., et al. 2003, *A&A*, 406, L63
- Fynbo, J. P. U., et al. 2009, *ApJS*, 185, 526
- Gehrels, N. 1986, *ApJ*, 303, 336
- Gehrels, N., Ramirez-Ruiz, E. & Fox, D. B., 2009, *ARA&A*, 47, 567
- Gunn, J. E., & Peterson, B. A., 1965, *ApJ*, 142, 1633
- Heger, A., et al. 2003, *ApJ*, 591, 288
- Heger, A., Langer, N., & Woosley, S. E. 2000, *ApJ*, 528, 368
- Hinshaw, G., et al. 2012, *arXiv*: 1212.5226
- Hjorth, J., et al. 2003, *Nature*, 423, 847
- Hopkins, A. M. 2004, *ApJ*, 615, 209
- Hopkins, A. M., & Beacom, J. F. 2006, *ApJ*, 651, 142
- Inoue, A. K., et al. 2005, *A&A*, 435, 471
- Inoue, S., Omukai, K., & Ciardi, B. 2007, *MNRAS*, 380, 1715
- Ishida, E. E. O., de Souza, R. S. & Ferrara, A. 2011, *MNRAS*, 418, 500
- Johnson, J. L., Dalla Vecchia, C. & Khochfa, S. 2013, *MNRAS*, 428, 1857
- Kewley L. & Kobulnicky H. A., 2007, in de Jong R. S., ed., *Island Universes: Structure and Evolution of Disc Galaxies*. Springer-Verlag, Dordrecht, p. 435
- Kistler, M. D., Yüksel, H., Beacom, J. F. & Stanek, K. Z. 2008, *ApJ*, 673, L119
- Kistler, M. D., Yüksel, H., Beacom, J. F., Hopkins, A. M. & Wyithe, J. S. B. 2009, *ApJ*, 705, L104
- Kistler, M. D., Yüksel, H., & Hopkins, A. M. 2013, *arXiv*: 1305.1630
- Komatsu, E., et al. 2011, *ApJS*, 192, 18
- Lamb, D. Q., & Reichart, D. E. 2000, *ApJ*, 536, 1
- Langer, N. 1998, *A&A*, 329, 551
- Langer, L., & Norman, C. A. 2006, *ApJ*, 638, L63
- Le, T., & Dermer, C. D. 2007, *ApJ*, 661, 394
- Li, L. X. 2008, *MNRAS*, 388, 1487
- MacFadyen, A. I., Woosley, S. E., & Heger, A. 2001, *ApJ*, 550, 410
- Madau, P., Haardt, F., & Rees, M. J. 1999, *ApJ*, 514, 648
- Maeder, A., & Meynet, G. 2000, *ARA&A*, 38, 143
- McQuinn, M., et al. 2008, *MNRAS*, 388, 1101
- Mészáros, P. & Rees, M. J. 2010, *ApJ*, 715, 967
- Mokiem, M. R., de Koter, A., Evans, C. J., et al. 2006, *A&A*, 456, 1131
- Oesch, P. A., Bouwens, R. J., Illingworth, G. D., et al. 2013, *arXiv*:1301.6162
- Panther, B., Heavens, A. F., & Jimenez, R. 2004, *MNRAS*, 355, 764
- Pawlik, A., Schaye, J. & van Scherpenzeel, E., 2009, *MNRAS*, 394, 1812
- Peimbert, M., Luridiana, V., & Peimbert, A. 2007, *ApJ*, 666, 636
- Planck Collaboration XVI. 2013, submitted to *A&A*
- Porciani, C. & Madau, P. 2001, *ApJ*, 548, 522
- Qin, S. F., Liang, E. W., Lu, R. J., Wei, J. Y. & Zhang, S. N. 2010, *MNRAS*, 406, 558
- Raskin, C., Scannapieco, E., Rhoads, J., & Della Valle, M. 2008, *ApJ*, 689, 358
- Robertson, B. E. & Ellis, R. S. 2012, *ApJ*, 744, 95
- Robertson, B. E., Ellis, R. S., Dunlop, J. S., McLure, R. J., & Stark, D. P. 2010, *Nature*, 468, 49
- Salpeter, E. E. 1955, *ApJ*, 121, 161
- Salvaterra R. & Chincarini G., 2007, *ApJ*, 656, L49
- Savaglio, S., 2006, *New J. Phys*, 8, 195
- Savaglio, S., et al. 2005, *ApJ*, 635, 260
- Schaefer, B. E. 2007, *ApJ*, 660, 16
- Stanek, K. Z., et al. 2003, *ApJ*, 591, L17
- Svensson, K. M., et al. 2010, *MNRAS*, 405, 57
- Tanvir, N. R., et al., 2004, *MNRAS*, 352, 1073
- Tegmark, M., Silk, J., Rees, M. J., Blanchard, A., Abel, T., & Palla, F. 1997, *ApJ*, 474, 1
- Thöne, C. C., et al. 2008, *ApJ*, 676, 1151
- Totani, T. 1997, *ApJ*, 486, L71
- Virgili, F. J., Zhang, B., Nagamine, K. & Choi, J. H. 2011, *MNRAS*, 417, 3025
- Wanderman, D., & Piran, T. 2010, *MNRAS*, 406, 1944
- Wang, F. Y., Bromm, V., Greif, T. H., Stacy, A., Dai, Z. G., Loeb, A. and Cheng, K. S. 2012, *ApJ*, 760, 27
- Wang, F. Y., & Dai, Z. G. 2009, *MNRAS*, 400, L10
- Wang, F. Y., & Dai, Z. G. 2011, *ApJ*, 727, L34
- Wang, F. Y., Qi, S. & Dai, Z. G. 2011, *MNRAS*, 415, 3423
- Wijers, R. A. M. J., Bloom, J. S., Bagla, J. S. & Natarajan, P. 1998, *MNRAS*, 294, L13
- Woosley, S. E. 1993, *ApJ*, 405, 273
- Woosley, S. E. & Heger, A. 2006, *ApJ*, 643, 914
- Wyithe, J. S. B. & Loeb, A., 2003, *ApJ*, 586, 693
- Yoon, S. C. & Langer, L., 2005, *A&A*, 443, 643
- Yoon, S. C., Langer, L. & Norman, C., 2006, *A&A*, 460, 199
- Yoshida, N., Abel, T., Hernquist, L., Sugiyama, N. 2003, *ApJ*, 592, 645
- Yüksel, H., Kistler, M. D., Beacom, J. F. & Hopkins, A. M. 2008, *ApJ*, 683, L5
- Yu, Y. W. et al., 2012, *JCAP*, 07, 023
- Zitouni, H. et al. 2008, *MNRAS*, 386, 1597

